iScience

CellPress
OPEN ACCESS

Article

Loss of histone reader Phf7 leads to immune pathways activation via endogenous retroviruses during spermiogenesis

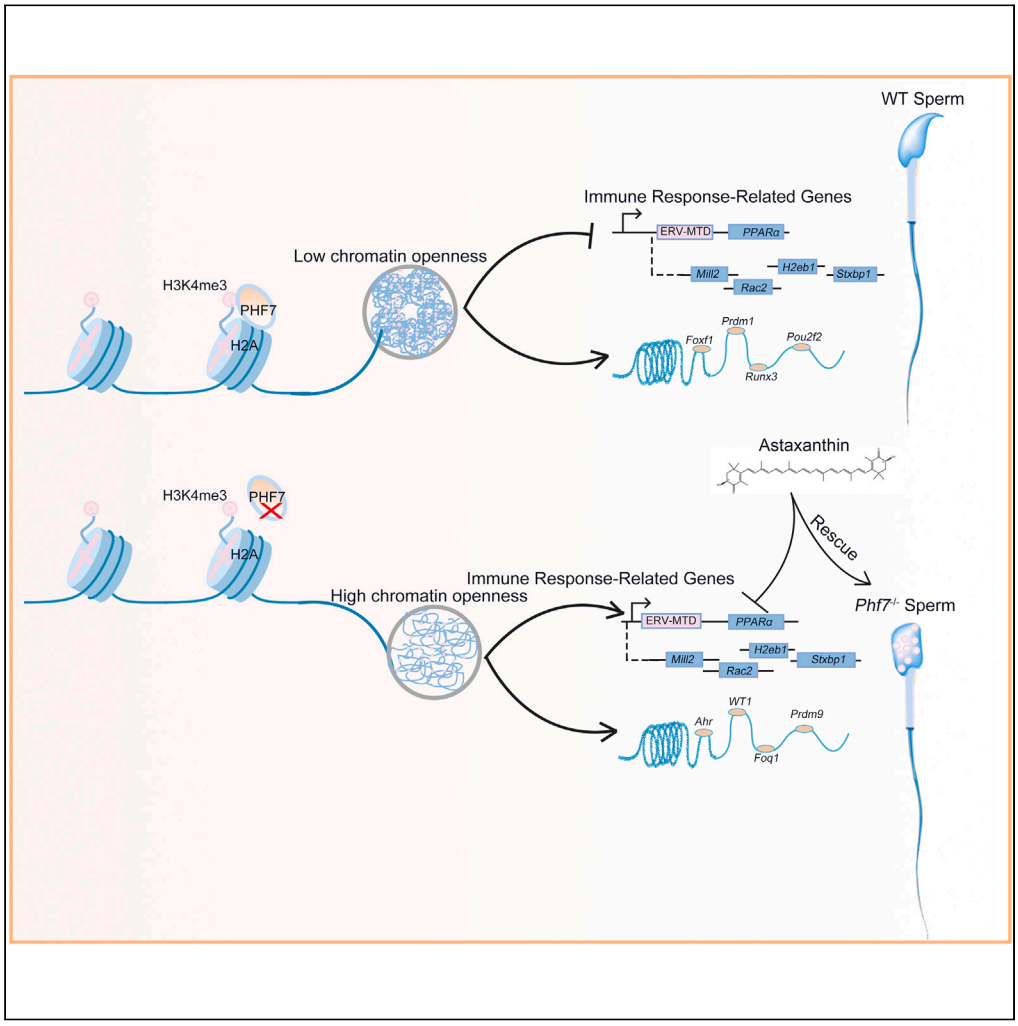

Jianxing Cheng, Tongtong Li, Zhongjie Zheng, ..., Hui Jiang, Wenming Xu, Haocheng Lin

jianghui55@163.com (H.J.)
xuwenming@scu.edu.cn (W.X.)
haochenglin292@163.com (H.L.)

Highlights

Phf7 is a target in human infertility and an epigenetic reader

The loss of Phf7 activates immune pathways via endogenous retrovirus

PPARα is an emerging target of immunity and inflammation in the testis

Astaxanthin is a promising drug for treating male infertility

Cheng et al., iScience 26, 108030
November 17, 2023
https://doi.org/10.1016/j.isci.2023.108030

iScience

CellPress
OPEN ACCESS

Article

Loss of histone reader Phf7 leads to immune pathways activation via endogenous retroviruses during spermiogenesis

Jianxing Cheng,[1,2,7] Tongtong Li,[3,7] Zhongjie Zheng,[1,2,7] Xueguang Zhang,[3] Mengyang Cao,[1,2] Wenhao Tang,[1,2,4] Kai Hong,[1,2] Rui Zheng,[3] Jichun Shao,[5] Xiaomiao Zhao,[6] Hui Jiang,[1,2,*] Wenming Xu,[3,*] and Haocheng Lin[1,2,8,*]

SUMMARY

Genetic studies have elucidated the critical roles of Phf7 in germline development in animals; however, the exact etiology of Phf7 mutations leading to male infertility and the possibility of mechanism-based therapy are still unclear and warrant further investigation. Using the Phf7 knockout mouse model, we verified that genetic defects were responsible for male infertility by preventing histone-to-protamine exchange, as previously reported. The deficiency of spermatogenesis caused by Phf7 deletion through the endogenous retrovirus-mediated activation of the immune pathway is a common mechanism of infertility. Furthermore, we identified PPARα as a promising target of immunity and inflammation in the testis, where endogenous retroviruses are suppressed, and Phf7 as a crucial regulator of endogenous retrovirus-mediated immune regulation and revealed its role as an epigenetic reader. The loss of Phf7 activates immune pathways, which can be rescued by the PPARα agonist astaxanthin. These results showed that astaxanthin is a potential therapeutic agent for treating male infertility. The findings in our study provide insights into the molecular mechanisms underlying male infertility and suggest potential targets for future research and therapeutic development.

INTRODUCTION

Spermatogenesis involves different stages, including premeiotic divisions, meiosis, and spermiogenesis. One of the key characteristics of spermatogenesis is histone-protamine replacement.[1] A recent study showed that histone modification, especially histone ubiquitination, constitutes a major epigenetic change in the transcription of post-meiotic genes required for spermiogenesis.[2] There are several genes, including RNF8, HIWI, and SCML2, are involved in histone ubiquitination during spermiogenesis, as demonstrated in a mouse knockout model.[3–5] However, apart from the defect in human spermatogenesis caused by HIWI mutation, other candidate genetic changes related to ubiquitination in patients with azoospermia have not been reported.

Phf7 (NYD-SP6) is a specific E3 ligase in humans and mice that is highly expressed in the testis, and its homolog is critical to promoting male sexual determination in the Drosophila germline.[6,7] Phf7-mediated H3K9me acts as a conserved epigenetic reader regulating germ cell identity during female germ cell development.[8] A recent study found that Phf7 is an E3 ligase of H2A ubiquitination and the deletion of Phf7 leads to abnormal H2A ubiquitination in sperm cells, which then damages the exchange of histone and protamine in the late stage of spermatogenesis, leading to infertility in male mice.[9] However, its specific role in mammalian spermatogenesis is poorly understood.

Endogenous retroviruses (ERVs) are remnants of exogenous retroviruses (proviruses) that have been integrated into the germline genome.[10] Transposable Elements (TE) with long terminal repeats are common features of ERVs and exogenous retroviruses, accounting for approximately 10% of the mammalian genome.[11] ERVs play essential roles in spermatogonia proliferation, meiosis, and other processes. For example, ERVs influence species-specific germline transcriptomes after the mitosis-to-meiosis transition in male mice. Specific ERVs

[1]Department of Urology, Peking University Third Hospital, Peking University, Beijing, China
[2]Department of Reproductive Medicine Center, Peking University Third Hospital, Peking University, Beijing, China
[3]Department of Obstetrics/Gynecology, Key Laboratory of Obstetric, Gynecologic and Pediatric Diseases and Birth Defects of Ministry of Education, West China Second University Hospital, Sichuan University, Chengdu 610041, China
[4]Department of Human Sperm Bank, Peking University Third Hospital, Peking University, Beijing, China
[5]Department of Urology, Second Affiliated Hospital of Chengdu Medical College (China National Nuclear Corporation 416 Hospital), Chengdu, Sichuan, China
[6]Department of Reproductive Medicine, Guangdong Provincial People's Hospital (Guangdong Academy of Medical Sciences), Southern Medical University, 106 Zhongshan 2nd Road, Guangzhou 510080, China
[7]These authors contributed equally
[8]Lead contact
*Correspondence: jianghui55@163.com (H.J.), xuwenming@scu.edu.cn (W.X.), haochenglin292@163.com (H.L.)
https://doi.org/10.1016/j.isci.2023.108030

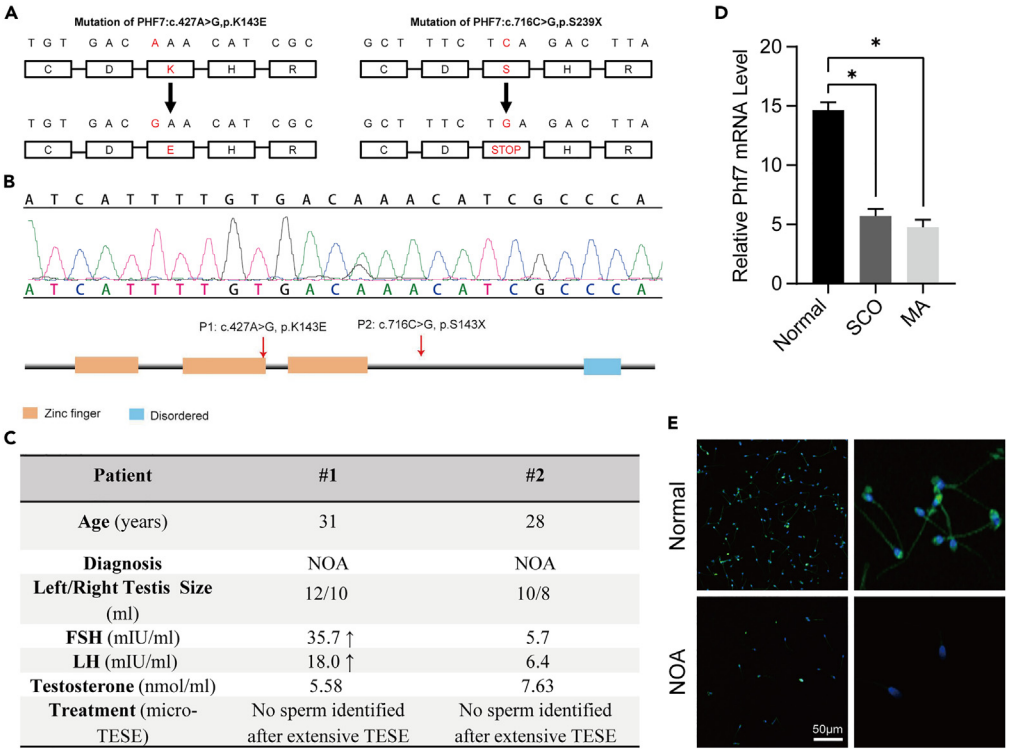

C

Patient	#1	#2
Age (years)	31	28
Diagnosis	NOA	NOA
Left/Right Testis Size (ml)	12/10	10/8
FSH (mIU/ml)	35.7 ↑	5.7
LH (mIU/ml)	18.0 ↑	6.4
Testosterone (nmol/ml)	5.58	7.63
Treatment (micro-TESE)	No sperm identified after extensive TESE	No sperm identified after extensive TESE

Figure 1. Validation of the pathogenic Phf7 mutations using Sanger sequencing and decreased expression of Phf7 is a common manifestation of patients with non-obstructive azoospermia

(A) Comparison of the wild-type and mutated Phf7 proteins in patients detected and the analysis of conservative Phf7 sequences (dark).

(B) DNA sequencing results of mutation sites in patient #1. Regarding the locations of the mutations, the first patient had a mutation located in the second zinc finger domain, and the second patient had a stop codon mutation located outside the functional domain.

(C) Clinical Presentation of two patients with mutations in Phf7.

(D) Relative expression levels of Phf7 mRNA by qPCR. Results from the control (n = 6), Sertoli cell-only syndrome patients (n = 7), and mature arrest patients (n = 7). Two-tailed unpaired Student's t test was used for the comparison of the mean values between two groups. Data are presented as the mean ± SD for each group and Significant differences were defined as *p < 0.05.

(E) Immunostaining images of Phf7 in human haploid sperm of patients with oligospermia and normal male. Phf7 was stained in green and nuclei were stained with DAPI (blue); the left panel is 10× magnification, the right panel is the enlarged picture showing the staining result.

function as active enhancers to drive germline genes, including a mouse-specific gene set, and bear binding motifs for critical regulators of spermatogenesis, including A-MYB.[12] However, the specific functions of ERVs in spermatogenesis remain largely unknown.

In the current study, we identified two Phf7 heterozygous mutations in a group of patients with azoospermia and demonstrated that Phf7 is a potential etiological factor in patients with non-obstructive azoospermia. Using Phf7-knockout mice constructed with CRISPR-Cas9 technology, we demonstrated that genetic defects are responsible for male infertility, preventing histone-to-protamine exchange during late spermiogenesis, as previously reported.[9] In addition, we discovered that the up-regulation via ERV-mediated "immune pathway" shared the mechanism of infertility in Phf7 knockout mice. Moreover, our results demonstrated that PPARα is an emerging target of immunity and inflammation in the testis, which was suppressed by ERV, and astaxanthin is a promising drug for treating male infertility.

RESULTS

Phf7 mutations were detected in patients with azoospermia

To determine whether Phf7 is involved in human spermatogenesis, we screened 40 patients with non-obstructive azoospermia (NOA) for potential mutations in Phf7. By sequencing the exons of Phf7 in the blood samples of all patients, we identified one heterozygous mutation, p.K143E (Figures 1A and 1B) and named it as patient 1. In addition, we accidentally found another mutation, p.S239X, using next-generation sequencing and named it as patient 2 (Figure 1A and Data S1). Both variants are nonsynonymous mutations, leading to the change of protein function. The first patient had a mutation located in the second zinc finger domain, and the second patient had a stop codon mutation located outside the functional domain. Besides two patients presented with similar clinical phenotype and patient 1 had elevated follicle-stimulating hormone and luteinizing hormone levels (Figure 1C). These findings suggested that mutations in Phf7 maybe related to male infertility. Furthermore, we found that the expression level of Phf7 in patients with NOA was significantly reduced in Sertoli cell-only and mature arrest

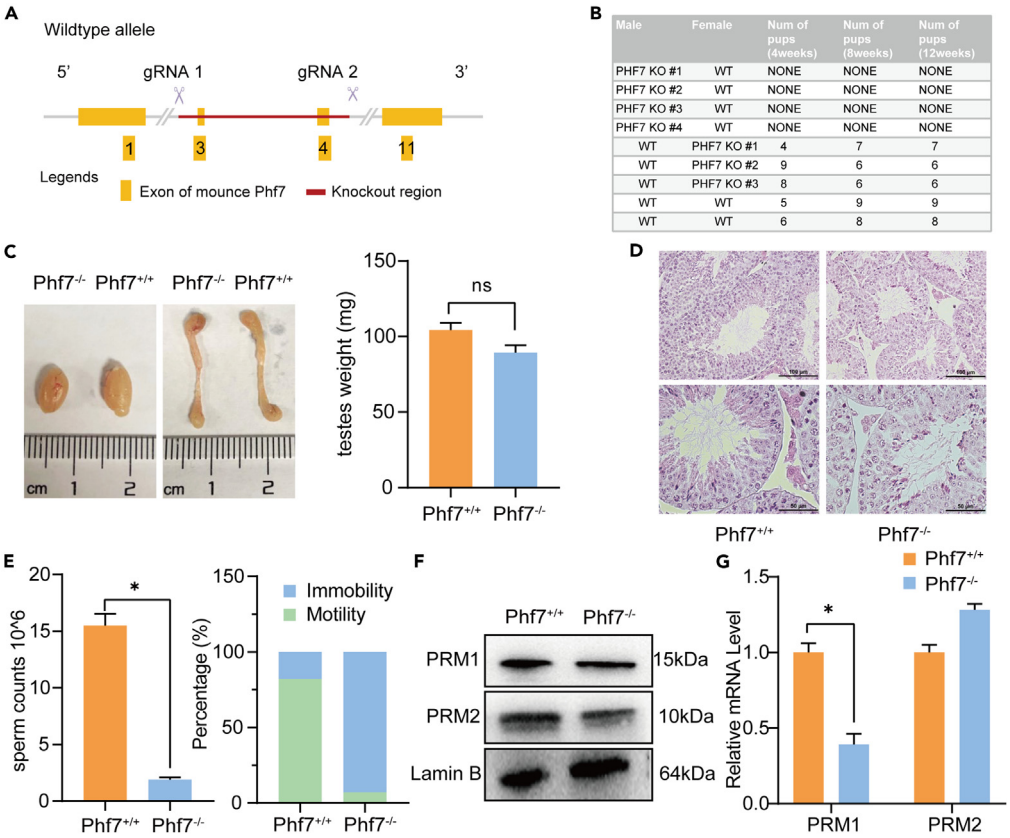

Male	Female	Num of pups (4weeks)	Num of pups (8weeks)	Num of pups (12weeks)
PHF7 KO #1	WT	NONE	NONE	NONE
PHF7 KO #2	WT	NONE	NONE	NONE
PHF7 KO #3	WT	NONE	NONE	NONE
PHF7 KO #4	WT	NONE	NONE	NONE
WT	PHF7 KO #1	4	7	7
WT	PHF7 KO #2	9	6	6
WT	PHF7 KO #3	8	6	6
WT	WT	5	9	9
WT	WT	6	8	8

Figure 2. Loss of Phf7 causes sterility in male mice with defective spermatogenesis at a later spermatogenic stage

(A) Schematic diagram for CRISPR-Cas9-mediated Phf7 knockout mice. Two sgRNAs were designed to target exons 3 and 4 of Phf7.

(B) Summary of the fertility test of Phf7 KO mice. All Phf7 KO male mice were infertile, while the females were fertile. Males were kept with females for 14 weeks since their sexual maturity.

(C) The testis and epididymis weight showed no significant change after Phf7 deletion.

(D) Hematoxylin and Eosin staining of testes sections from 10-week-old Phf7 WT and KO mice.

(E) Sperm counts in cauda epididymis from Phf7 KO and WT mice (n = 6). CASA assays of motility and immobility of sperm from 10-week-old mutant and wild-type mice.

(F) Western blot of PRM1 and PRM2 in sperm from 10-week-old Phf7 KO and WT mice with Lamin B as a loading control.

(G) Comparation of PRM1 and PRM2 RNA expression of 10-week-old Phf7 KO and WT mice testes using qPCR. Two-tailed unpaired Student's t test was used to compare the mean values between two groups. Data are presented as the mean ± SD for each group and Significant differences were defined as *p < 0.05.

two kind patients with NOA specifically (Figure 1D and S2), and Phf7 expression was lower than that in the control group, as confirmed by immunofluorescence (Figure 1E). These findings clearly indicated that Phf7 was involved in human male spermatogenesis, and the expression of Phf7 in patients with NOA was significantly reduced. We could not rule out other potential modifiers in the genome of mutant patients that may contribute to the expression of the disease phenotype, but the decreased expression of Phf7 was a common manifestation in patients with NOA in the current study.

Phf7 knockout mice showed male infertility

To investigate whether Phf7 mutations play a causative role in male infertility and elucidate the underlying mechanism, we constructed a Phf7$^{+/-}$ mouse model with frameshift mutations by injecting Cas9 mRNA, sgPhf7-A, and sgPhf7-B into zygotes with a C57BL/6 background. Two sgRNAs were designed to target exons 3 and 4 of Phf7 (Figures 2A, S2A, and S2B). While two sgRNAs (sgPhf7-A and sgPhf7-B) were designed to target exons 2 and 4 of Phf7 as shown in the previous article [9]. After obtaining these mice, Phf7$^{+/-}$ females were backcrossed with WT males, leading to stable mouse lines carrying the mutant Phf7$^{+/-}$. Knockout efficiency was confirmed using qPCR (Figure S2D). Homozygous Phf7 knockout mice were then obtained by crossing Phf7$^{+/-}$ mice. We found that all Phf7$^{-/-}$ males were sterile, whereas all Phf7$^{-/-}$ females exhibited normal fertility during cage breeding. We then counted the number of offspring of each genome type mice (Figure 2B).

Subsequently, we investigated the stage at which spermatogenesis failed in the Phf7$^{-/-}$ mice. The average weight of the testes from adult Phf7$^{-/-}$ mice was similar to that of the WT controls (Figure 2C), and histological analysis indicated that spermatocytes, round spermatids, and early elongating spermatids were unaltered (Figure 2D), whereas sperm harvested by dissecting the epididymis was strongly reduced in

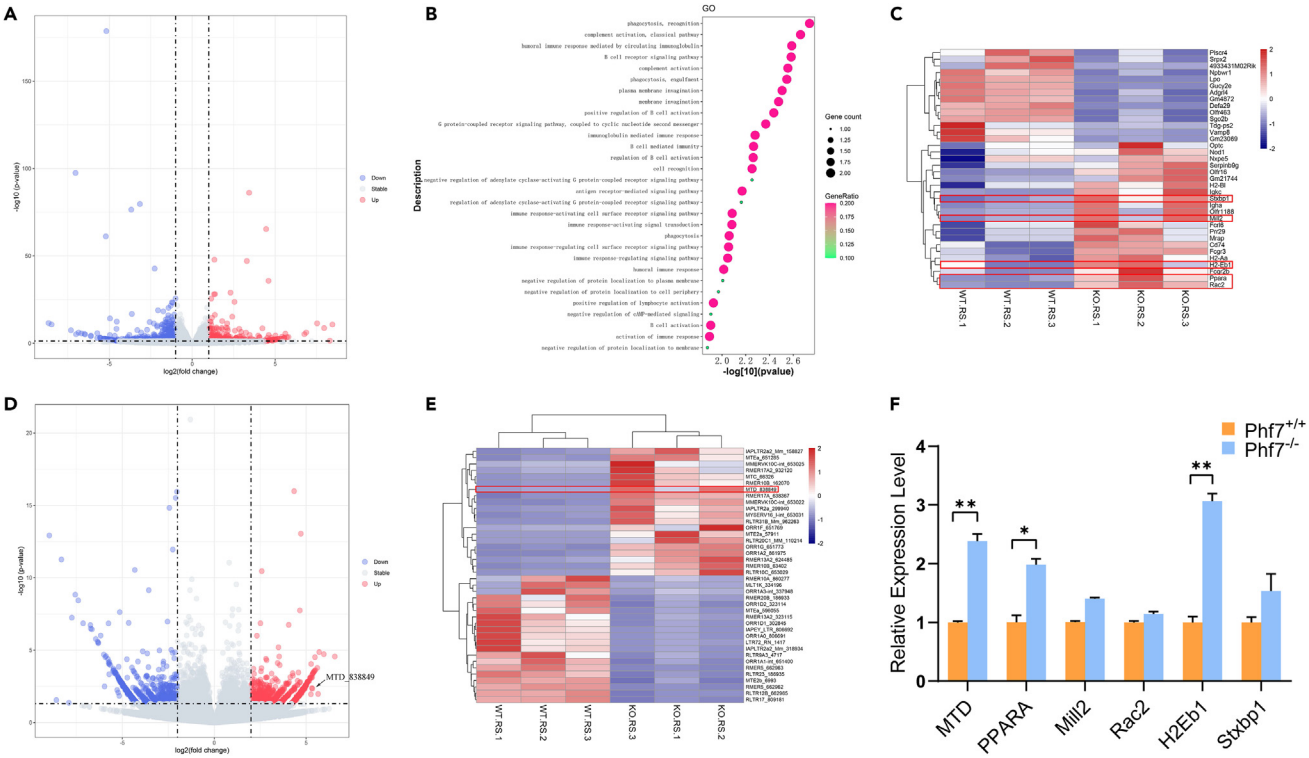

Figure 3. RNA-seq analysis of mouse testis round spermatids shows the enrichment of immune pathways and remodeling of ERV expression

(A) Volcano plot of differentially expressed genes in Phf7 KO round spermatids compared with those of WT. Red points represent significantly up-regulated and blue points represent significantly down-regulated genes in Phf7 KO with greater than 2.0-fold change.

(B) Some biological functions related to the 20 up-regulated genes compared with WT mice.

(C) Two-dimensional hierarchical clustering of distinguishable gene expression profiles.

(D and E) (D) Volcano plot of differentially expressed ERVs in Phf7 KO compared with wild-type mice. Red points represent significantly up-regulated and blue points represent significantly down-regulated genes in Phf7 KO with greater than 2.0-fold change (E) Heatmap showing the expression of differentially expressed ERVs. MTD-838849 is highlighted on the right-hand side.

(F) Real-time PCR showing differentially expressed genes in Phf7 KO mice. All quantitative biochemical data were representative of at least three independent experiments. A two-tailed unpaired Student's t-test was used to compare the mean values between two groups. Data are presented as mean ± SD for each group, and significant differences were defined as *$p < 0.05$, **$p < 0.01$.

Phf7$^{-/-}$ mice. CASA showed that the percentage of immotile sperm in Phf7$^{-/-}$ mice was significantly increased (Figure 2E). Thus, we proposed that the loss of Phf7 could cause defective spermatogenesis at a later spermatogenic stage. Western blotting and real-time PCR showed that the expression of PRM1 and PRM2 in the sperm was significantly decreased in Phf7$^{-/-}$ mice (Figures 2F and 2G). These results demonstrated that the deletion of Phf7 results in a significantly compromised spermiogenesis process, which was consistent with the results of previous studies.[9,13] By replicating the disease phenotype in a mouse model, these results suggested that primitive mutations may be the driving factor of human diseases.

Phf7 deletion causes the activation of immune pathways and remodeling of endogenous retroviruses expression

Previous studies have shown that mutations in Phf7 can cause H2A ubiquitination and alteration of H3K4me2/me3.[6] As both histone modifications are mainly involved in transcriptional regulation, we analyzed previously published RNA-seq data by Wang et al.[9] to compared the transcriptional changes after Phf7 deletion. The targeted exons were not consistent; however, the knockout fragments overlapped. In addition, the phenotypes of Phf7 knockout mice were consistent. Therefore, previous transcriptome datasets were largely same to our own. The volcano plot showed that the deletion of Phf7 resulted in 385 upregulated genes and 530 downregulated genes (Figure 3A). GO analysis showed that the upregulated genes were mainly enriched in complement activation, classical pathway, humoral immune response mediated by circulating immunoglobulin, and B cell receptor signaling pathways, among others (Figure 3B). Two-dimensional hierarchical clustering of distinguishable gene expression profiles displays specific immune-related genes (Figure 3C). Gene enrichment analysis showed that the downregulated genes enrich biological processes such as the regulation of cell growth and Wnt signaling pathways. These results showed that the "immune pathway" was among the most significant enrichment pathways (Figure S3A).

During spermatogenesis, germ cells undergo massive cellular reconstruction and dynamic chromatin remodeling to facilitate highly diverse transcriptomes that are required for the production of functional sperm.[14] Recent studies have shown that ERVs are a major driving force for the rapid evolution of mammalian genes.[15] Genes regulated by ERV can be adjacent to ERV and can affect immune response, placental development, and embryonic development process. Therefore, we analyzed changes in ERV expression after Phf7 deletion. Our results showed that 955 ERVs were upregulated, and 926 ERVs were downregulated, two-dimensional hierarchical clustering of distinguishable gene expression profiles displays specific immune-related ERVs (Figures 3D and 3E). These findings indicated a significant dysregulation of ERVs. Subsequently, we performed a coverage analysis on the differentially expressed ERVs to study the relationship between the expression changes of ERVs and adjacent genes (Figure S3B). We found that the enriched "immune pathways" were most significantly affected by the upregulation of ERV-MTD (Figures S3C and S3D), and these enriched "immune pathway" genes were shown (Data S2). Subsequently, we examined the expression of ERV-MTD and its affected genes in the testes of Phf7$^{-/-}$ mice, including PPARα, H2Eb1, Mill2, Rac2, and Stxbp1. Quantitative PCR results showed that ERV-MTD was significantly increased in the testes of Phf7$^{-/-}$ mice, and PPARα and H2Eb1 expression was also increased significantly (Figure 3F). In addition, western blotting demonstrated that PPARα expression in the testes of Phf7$^{-/-}$ mice was upregulated (Figure S4A). These results indicated that Phf7 mutation increased the expression of ERV-MTD and "immune pathway" genes.

Endogenous retroviruses-MTD might suppress the expression of "immune pathway" genes

Recent studies have shown that ERVs are critically involved in the regulation of spermatogenesis[12]; therefore, we focused on the function of ERV-MTD. We investigated whether ERV-MTD controls spermatogenesis *in vitro*. We designed gRNAs targeting ERV-MTD, constructed Cas-9 lentivirus (Figures 4A and S5A), and transfected them into GC1 and GC2 cells. We established two ERV-MTD knockout germline cells with 760 or 1015 bp deletion including ERV-MTD (Figures 4B, 4C, and S5B). We found that the morphology was altered, and cell proliferation was reduced after ERV-MTD deletion (Figures 4D and 4E). Subsequently, we examined the expression of PPARα after the deletion of ERV-MTD. Our results showed that the deletion of ERV-MTD downregulated PPARα expression (Figures 4F and 4G). In addition, the expression of "immune pathway" genes, including Mill2, Rac2, and H2Eb1 also decreased (Figure 4H). These results suggested that ERV-MTD may play a key role in spermatogenesis by suppressing "immune pathway" genes.

Metabolism of testicular germline cells changed after Phf7 mutation

Given that Phf7 functions as a histone code reader that binds methylated histone H3 (H3K4me2/me3) and controls gene expression programs, we attempted to understand the underlying transcriptional chromatin accessibility of Phf7 using ATAC-seq. The IDR was used to test and analyze the reproducibility between replicates. We used DiffBind to identify significantly differentially bound sites using ATAC-seq data. We identified 6,139 differentially bound sites (Figure 5A, fold change $\geq$2, FDR $\leq$0.01). Our results showed that the mutation of Phf7 resulted in more open chromatin of cells in the testis, and the peaks occupied a wide region in the promoter (Figures 5A and 5B). GO enrichment analysis revealed that DNA repair was the most significantly enriched pathway among the differentially expressed peaks (Figure 5C). Furthermore, peaks were found to be enriched in the "neurodevelopmental" pathway in the WT mice while the peaks of Phf7$^{-/-}$ group were enriched in the "ketone metabolism" pathway (Figures 5D and 5E), suggesting that the metabolism of testicular germ cells changed after Phf7 mutation. In addition, the shared common processes between spermatogenesis and neurodevelopment confirmed the reliability and authenticity of our sequencing data.

Furthermore, we used both ChIP-seq and ATAC-seq to determine whether the expression was related to the shift in epigenetic regulation from normal regulation to immune-related gene regulation (Figures S6A and S6B). Motif analysis showed that the Ahr motif was most significantly enriched within the Phf7$^{-/-}$ group (Figure 5F). Ahr is a transcription factor enriched in the PPARα pathway,[16] and our results showed that mice harboring Phf7 deletion displayed the upregulation of Ahr and PPARα in the testis (Figure S4A). This result demonstrated that increased Ahr binding may be involved in the regulation of the PPARα-related pathway. However, whether this regulation is dependent or independent of MTD is unclear. Furthermore, GO pathway analysis of the best-matched genes with calling motifs in Phf7$^{-/-}$ ATAC-seq showed that several pathways were activated, including sex differentiation, cell fate determination, reproductive structure development, and reproductive system development, indicating that proliferation-related pathways were activated after the deletion of Phf7 (Figures S6C, S6D, and S6E). Besides, bioinformatic analysis showed that PPARα is a potential target gene regulated by ERV-MTD (Figure S6F).

Astaxanthin partially rescued the sperm count and motility of Phf7$^{-/-}$mice

PPARα regulates spermatogenesis, and its key role in spermiogenesis has been well established in previous studies.[17,18] Astaxanthin is a PPARα modulator that has been shown to have anti-inflammatory and anti-oxidative properties.[19,20] It has been widely used to treat diseases related to oxidative stress.[21] Since the transcriptome and *in vitro* studies showed that immune pathways are the major downstream pathways activated by the deletion of Phf7, we examined the therapeutic effect of astaxanthin on Phf7$^{-/-}$ mice. For the *in vivo* study, Phf7$^{-/-}$ mice were gavaged with astaxanthin for 4 weeks, while the control mice were treated with the same volume of solution (six replicates per treatment). We found that astaxanthin significantly increased sperm count and motility (Figures 6A and 6B). In addition, experiments revealed that the addition of astaxanthin resulted in reduced ROS levels and germ cell apoptosis (Figures 6C–6E) in the testis. These results indicated that astaxanthin can partially rescue the spermatogenesis defects caused by Phf7 deletion. Thus, our results suggested that PPARα is a promising target that can be explored using astaxanthin and other drugs targeting the PPARα pathway.

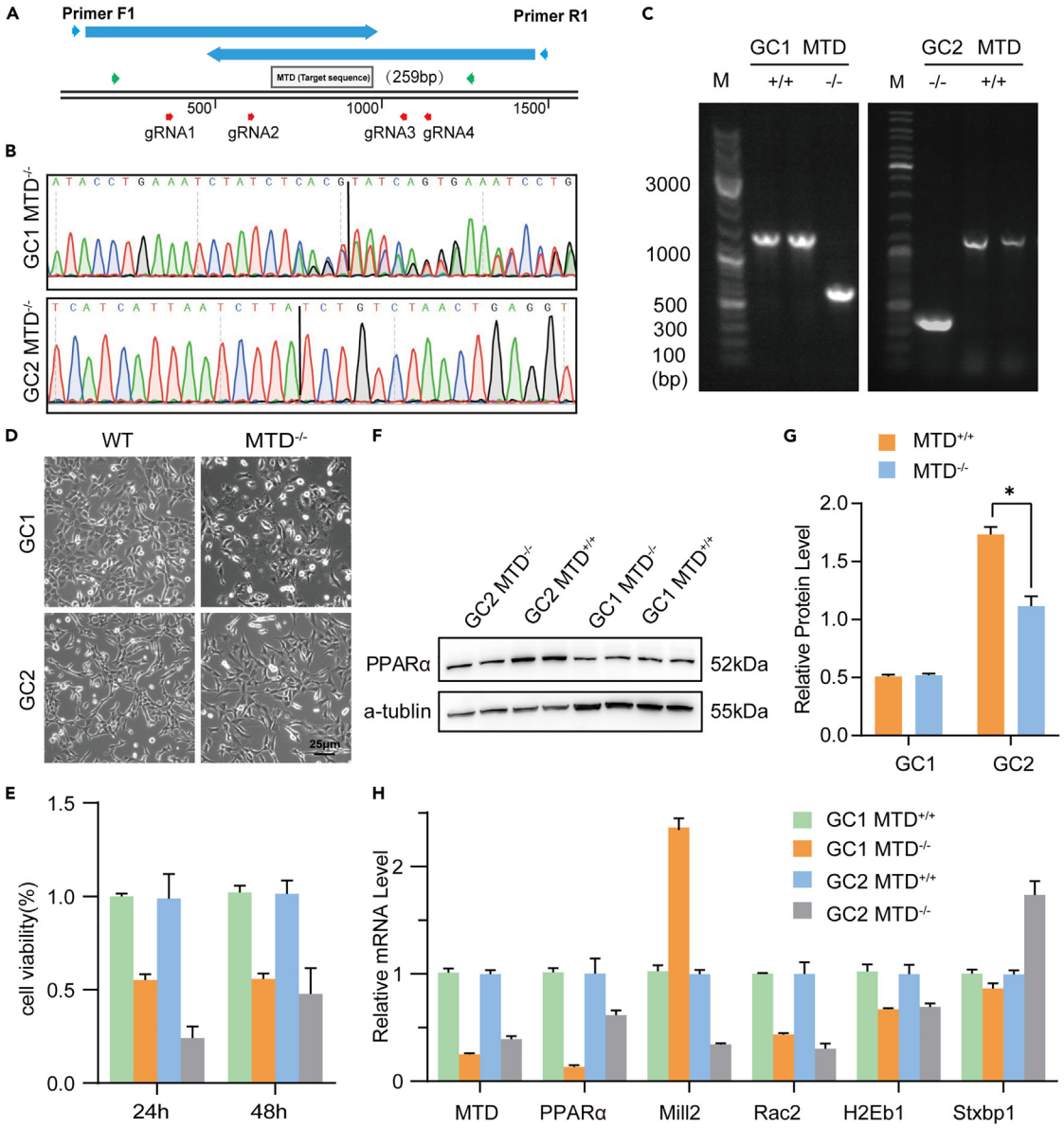

Figure 4. Germline cells decreased the expression of "immune pathways" genes after ERV-MTD knockout

(A) Schematic diagram showing CRISPR/Cas9-mediated deletion of ERV-MTD using four sgRNAs.

(B) DNA sequencing results of mutation sites in two germline cells.

(C) Validation of two MTD$^{-/-}$ germline cells (GC1 and GC2) by genomic DNA PCR with primers. M, DNA marker.

(D) Cell morphology was changed after the deletion of MTD, including GC-1 and GC-2 cells. Scale bar, 100 μm.

(E) Results of CCK-8 assays indicated that the depletion of MTD significantly decreased the proliferation of spermatogenic cells.

(F) Western blot analysis of PPARα protein in WT and MTD$^{-/-}$ spermatogenic cells. α-Tubulin was used as a loading control.

(G) Relative gray scale of PPARα expression determined following WB analysis.

(H) The expression levels of MTD, PPARα, and Rac2 after MTD depletion in GC1 and GC2 cells were significantly decreased, as measured by qPCR and normalized to β-Actin levels. All quantitative biochemical data were representative of at least three independent experiments. Two-tailed unpaired Student's t test was used to compare the mean values between two groups. Data are presented as the mean ± SD for each genotype and significant differences were defined as *$p < 0.05$, **$p < 0.01$.

The expression levels of Phf7 were downregulated, whereas those of PPARα and MTD were significantly upregulated in patients with NOA (Figures S7A and S7B), indicating that the regulatory pathway also regulates human spermatogenesis. ChIP-qPCR was conducted in testes of mice to validate the binding sites, revealing that PHF7 could regulate PPARα transcription by binding to the specific locations on the ERV-MTD region, while decreased binding in the Phf7 knockout mice. The results of ChIP-seq showed that almost PHF7-binding peaks overlapped

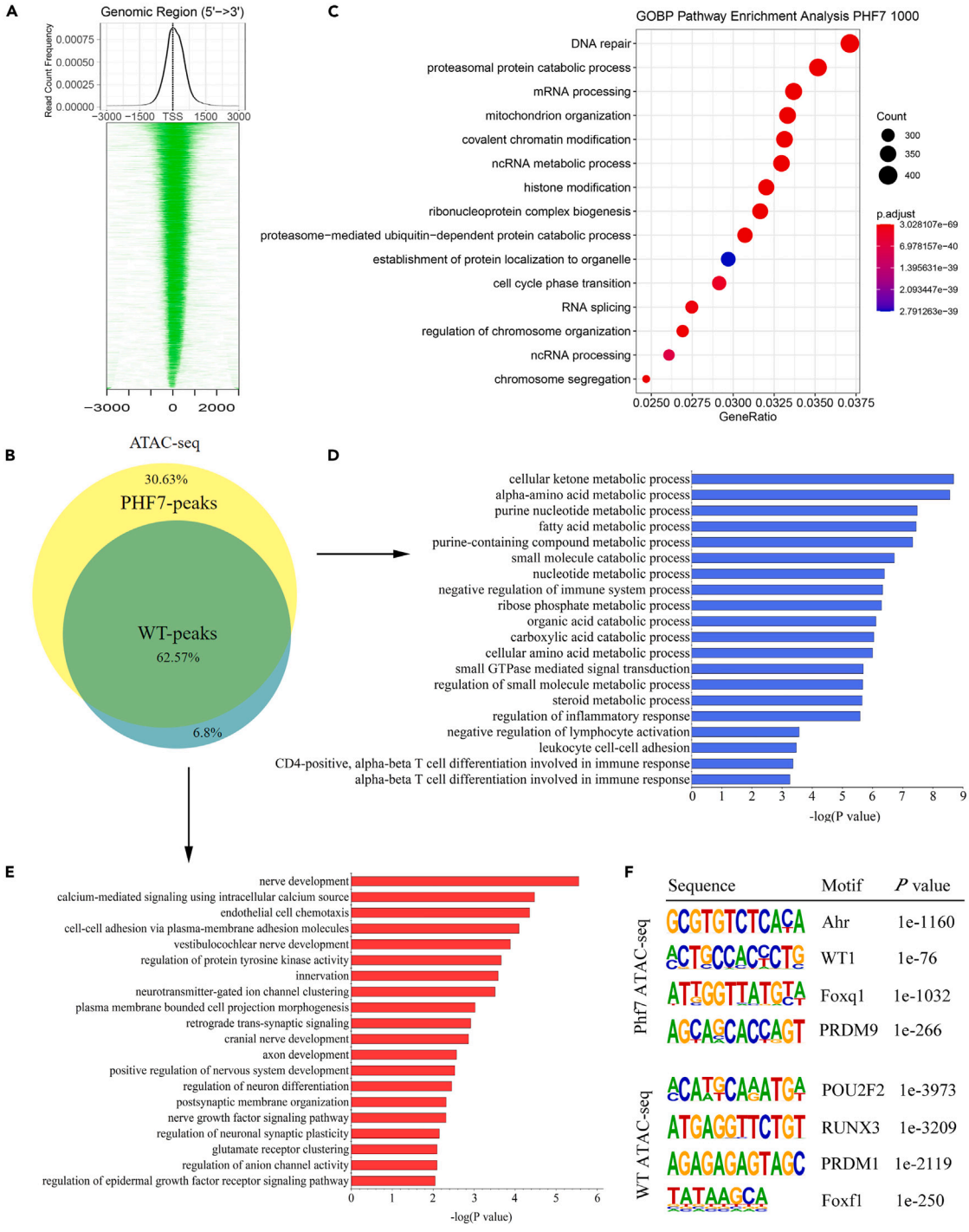

Figure 5. ATAC-seq analysis of mouse testis

(A) Heatmap and density plot of differential Phf7 ATAC-seq peaks (±3 kb window centered on the peak summit). n = 2 biologically independent replicates per group.

(B) Venn diagram shows differential peaks between Phf7 and WT were determined in ATAC-seq.

(C) GO pathway analysis of differential peak annotated genes.

(D) GO pathway analysis of regions with peaks in the absence of Phf7 as determined by clusterProfiler.

(E) GO analysis shows the significantly enriched pathway in the WT ATAC-Seq analysis," Nerve development" was the most significantly enriched pathway.

(F) Motif analysis indicated that Ahr, WT1, FoxQ1, and PRDM1 were significantly enriched after Phf7 deletion, while in WT testis, Pou2f2, Runx3, PRDM1, and FoxF1 were significantly enriched.

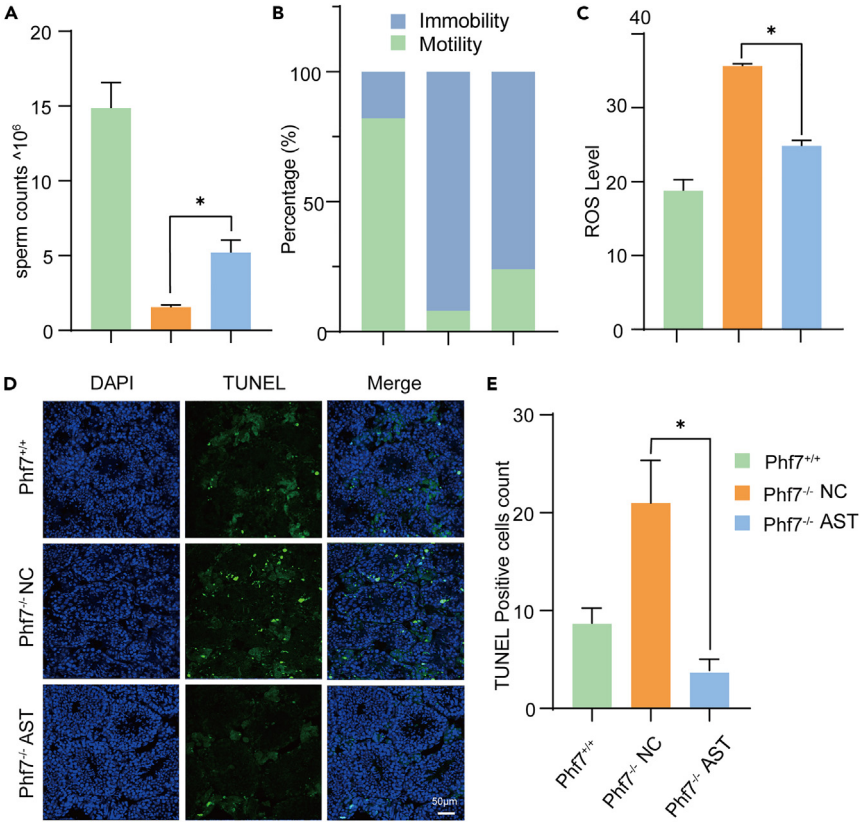

Figure 6. Astaxanthin improves sperm motility and reduced reactive oxygen species (ROS) levels and germ cell apoptosis

(A) Sperm counts in cauda epididymis from Phf7 KO and WT mice. (n = 6).

(B) CASA assays of motility and immobility percentage of sperm from cauda of 10-week-old mutant and wild-type mice after a month astaxanthin treatment.

(C) Astaxanthin decreased sperm ROS generation. ROS level as quantified in the Phf7 KO testis.

(D) TUNEL assay of testis sections from astaxanthin treated mice. Testis sections were stained with TUNEL (green) to indicate apoptosis cells. Nuclei were stained with DAPI (blue).

(E) Quantification of the seminiferous tube with a positive TUNEL signal in the testis. Two-tailed unpaired Student's t test was used to compare the mean values between two groups. Data are presented as the mean ± SD for each genotype and significant differences were defined as *p < 0.05, **p < 0.01.

with those of H3K4me3, providing supporting evidence for the specific binding of PHF7 to H3K4me3. So H4K4me3 ChIP-qPCR was conducted in testes to validate the effect of PPARα agonist Astaxanthin on chromatin state. We found H4K4me3 association is reduced after the treatment of astaxanthin in the Phf7$^{-/-}$ mouse for most of the ERV-MTD analyzed. Indicated the activated immune pathways were suppressed (Figures S8A and S8B).

DISCUSSION

Patients with azoospermia constitute more than 1% of the general population; however, the only gene with recurrent mutations detected in non-obstructive azoospermia is TX11.[22,23] Liu et al. recently reported that two heterozygous mutations in PIWI genes lead to spermiogenesis defects caused by the blocked shuttling of RNF8 from the cytoplasm to the nucleus.[5] Phf7 is one of the early identified genes responsible for histone H2A ubiquitination, leading to the compromised transition of histones to protamine, resulting in spermiogenesis defects.[9] Therefore, the current study is the first to show that Phf7 mutations maybe related to the etiology of azoospermia. In addition, patients with NOA showed reduced expression of Phf7 at the RNA and protein levels. Moreover, we found that mice with Phf7 deletion had defects in the late stage of spermatogenesis, leading to male infertility, and these results are consistent with those of previous studies.[9,13] Although the mutations in the mouse model were not the same as those observed in human patients, our study provided insights into the potential role of Phf7 in male infertility and the molecular mechanisms underlying it. Further investigation is required to confirm the relevance of our findings to human biology.

ERVs are widely expressed in the testis, and the dysregulation of ERVs contributes to spermiogenesis defects in male infertile patients.[24,25] In the current study, our transcriptome analysis showed that the "immune pathways" were activated after Phf7 deletion and that ERV expression was altered simultaneously. Furthermore, overlap and GO analyses showed that ERVs can significantly activate immune pathways. Moreover, the *in vitro* results showed that ERV-MTD has an immunosuppressive function and plays a role in germ cell proliferation. Our results

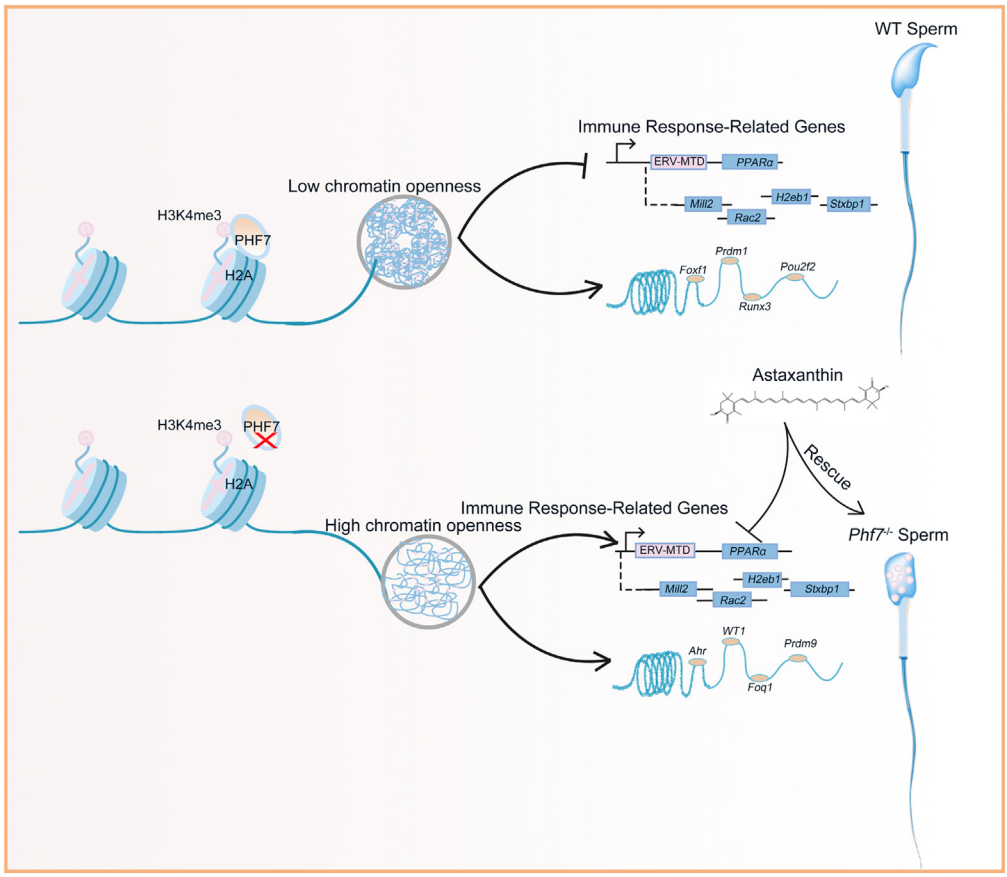

Figure 7. Mechanistic insights from the current study

The results show that PHF7, an epigenetic reader, is one of the factors causing human infertility. The loss of Phf7 causes more open chromatin in testicular cells and upregulation through ERV-mediated "immune pathways." Furthermore, the expression of PPARα was inhibited by ERV.

suggested that the crosstalk of H3K4me3 in Phf7 KO mice may regulate the ERV-MTD-mediated immune pathway, leading to defective spermatogenesis. However, further studies are needed to understand the molecular mechanisms underlying the deletion of Phf7-mediated transposable elements activation and their link to spermatogenesis. And some of the downregulated genes identified in the knockout model were related to the Wnt signaling pathway, which is known to play a role in cell growth and development. This also requires further extensive research.

Genetic studies have shown that Phf7 is a histone code reader that can specifically associate with H3K4me2/me3 and influence gene expression[6]; however, how Phf7 affects chromatin structure remains unclear. Our ATAC-seq results showed significantly altered chromatin accessibility after the deletion of Phf7. Compared with WT mice, GO analysis showed that DNA repair was the most significantly enriched pathway, indicating that Phf7 plays a role in DNA repair during spermiogenesis. Moreover, the enrichment pathway shifted from "neurodevelopment" to "ketone metabolic process," indicating that the metabolic process had changed. Furthermore, motif analysis showed that various transcription factors, including Ahr, were activated, and GO analysis showed that most transcription factors bind to germline cell proliferation, which corresponds to the key role of Phf7 in the epigenetic regulation of germ cells. A recent study showed that Phf7 is a critical factor in heart regulation as it plays a critical role in cardiac reprogramming.[26] Mechanistically, Phf7 reprogram fibroblasts to cardiomyocytes by binding to cardinal super-enhancers through cooperation with the SWI/SNF complex.[27] Our results showed that the epigenetic switch may be a common mechanism for the role of Phf7, and that the binding of Phf7 with histone modification markers, including H3K4, is critical for activating ERV-MTD transcription and metabolic activation (Figure 7).

Spermatogenesis is a complex process that mainly includes histone modification and flagellar development.[2,28,29] Few studies have established a functional link between histone modifications and immune pathway activation during spermiogenesis. In the current study, we showed that Phf7, an epigenetic reader, played a critical role in immune suppression during spermatogenesis. Our results showed that histone modification defects could cause abnormal immune pathway activation, which contributes to spermiogenesis defects, and anti-oxidation drugs, such as astaxanthin, can be promising drugs for treating patients with asthenospermia and oligospermia. Antioxidant drugs have been widely used in male infertility clinics.[30] Our results showed that PPARα is an emerging target of immunity and inflammation in the testis, and that astaxanthin is a promising drug for treating male infertility. However, its clinical efficacy remains controversial and requires further clinical data.

Limitations of the study

Our findings demonstrate that genetic mutations in the epigenetic reader Phf7 are a potential etiological factor in patients with NOA; however, our study has several limitations, and therefore it needs to be cautious to extend our conclusions on the mice data to human infertile cases directly. First, we found that the phenotypes of phf7 mutations in humans and mice are inconsistent. In humans, heterozygous mutations can cause azoospermia, whereas in mice, homozygous mutations are required to cause similar phenotypes. Second, the location of the human mutation was p.K143E and p. S239X found in our study, while the mice mutant location is different, indicating that the phenotypic result maybe different between mice and human cases. In addition, spermatogenesis deficiency caused by the deletion of Phf7 through ERV-mediated activation of the immune pathway is a common mechanism of infertility. However, whether the cause of these changes in ERV expression is because of the loss of E3 ligase H2A ubiquitination function or associated with H3K9me3 is unclear. Therefore, more research is needed to understand the epigenetic mechanism of Phf7 leading to ERV changes and the molecular mechanism of Phf7 and ERV-mediated testicular immune pathway activation.

STAR★METHODS

Detailed methods are provided in the online version of this paper and include the following:

- KEY RESOURCES TABLE
- RESOURCE AVAILABILITY
  - Lead contact
  - Materials availability
  - Data and code availability
- EXPERIMENTAL MODEL AND SUBJECT DETAILS
  - Animal use and care
  - Generation of ERV-MTD knockout cell lines
  - Human samples
- METHOD DETAILS
  - RNA extraction and reverse transcriptase polymerase chain reaction (RT-PCR)
  - Sperm isolation and computer-assisted sperm analysis (CASA)
  - Histology and immunohistochemical staining
  - Terminal deoxynucleotidyl transferase dUTP nick-end labeling (TUNEL) and reactive oxygen species (ROS)
  - Scanning electron microscopy
  - Immunofluorescence staining
  - Western blot analysis
  - ChIP-qPCR analysis
  - Assay for transposase-accessible chromatin using sequencing (ATAC-seq) analysis
  - RNA-seq analysis
  - Differential expression analysis
  - ERV analysis
- QUANTIFICATION AND STATISTICAL ANALYSIS

SUPPLEMENTAL INFORMATION

Supplemental information can be found online at https://doi.org/10.1016/j.isci.2023.108030.

ACKNOWLEDGMENTS

We thank Prof. Jiadong Wang (School of Basic Medical Sciences, Peking University Health Science Center) and Prof. Mo Li (Peking University Third Hospital) for their support and contributions to this project. We also thank Prof. Shang Lijun（London Metropolitan University）for proofreading of our article. This work was supported by the Natural Science Foundation of Beijing (General #7212134), National Natural Science Foundation of China (#81601272), Peking University Clinical Medicine +X Youth Special Program (PKU #2018LCXQ019), National Key Research and Development Program of China (2018YFC1003600),Peking UniversityClinical Scientist Training Program" and "the Fundamental Research Funds for the Central University（BMU2023PYJ H012）, National Natural Science Foundation of China (grant numbers 8227060392), Guangdong Basic and Applied Basic Research Foundation (2020B1515020001) and the GDPH supporting fund (KY012021439).

AUTHOR CONTRIBUTIONS

W.M.X., H. J., and T. T. L. designed and supervised the study. J.X.C., M.Y.C., and Z.J.Z. contributed to hypoxia treatment. J.C.S., W.H.T., and H.J. contributed to the cell culture, molecular biology work, and immunohistochemistry. L. T. T. and K. H. contributed to the bioinformatic analysis. J.X.C., T.T.L. and X.G.Z. drafted the initial article. H.J., Xiaomiao Zhao, H.C.L. and W.M.X. revised the article.

DECLARATION OF INTERESTS

The authors declare no competing or financial interests.

Received: December 8, 2022
Revised: April 12, 2023
Accepted: September 21, 2023
Published: September 25, 2023

REFERENCES

1. Blanco, M., and Cocquet, J. (2019). Genetic Factors Affecting Sperm Chromatin Structure. Adv. Exp. Med. Biol. *1166*, 1–28. https://doi.org/10.1007/978-3-030-21664-1_1.
2. Sheng, K., Liang, X., Huang, S., and Xu, W. (2014). The role of histone ubiquitination during spermatogenesis. BioMed Res. Int. *2014*, 870695. https://doi.org/10.1155/2014/870695.
3. Hasegawa, K., Sin, H.S., Maezawa, S., Broering, T.J., Kartashov, A.V., Alavattam, K.G., Ichijima, Y., Zhang, F., Bacon, W.C., Greis, K.D., et al. (2015). SCML2 establishes the male germline epigenome through regulation of histone H2A ubiquitination. Dev. Cell *32*, 574–588. https://doi.org/10.1016/j.devcel.2015.01.014.
4. Lu, L.Y., Wu, J., Ye, L., Gavrilina, G.B., Saunders, T.L., and Yu, X. (2010). RNF8-dependent histone modifications regulate nucleosome removal during spermatogenesis. Dev. Cell *18*, 371–384. https://doi.org/10.1016/j.devcel.2010.01.010.
5. Gou, L.T., Kang, J.Y., Dai, P., Wang, X., Li, F., Zhao, S., Zhang, M., Hua, M.M., Lu, Y., Zhu, Y., et al. (2017). Ubiquitination-Deficient Mutations in Human Piwi Cause Male Infertility by Impairing Histone-to-Protamine Exchange during Spermiogenesis. Cell *169*, 1090–1104.e13. https://doi.org/10.1016/j.cell.2017.04.034.
6. Yang, S.Y., Baxter, E.M., and Van Doren, M. (2012). Phf7 controls male sex determination in the Drosophila germline. Dev. Cell *22*, 1041–1051. https://doi.org/10.1016/j.devcel.2012.04.013.
7. Lu, Y., Huo, R., Yuan, Y., Li, J., Shi, Q., and Sha, J. (2006). Human testicular protein NYD-SP16 is involved in sperm capacitation and the acrosome reaction. Fertil. Steril. *86*, 1228–1234. https://doi.org/10.1016/j.fertnstert.2006.05.025.
8. Smolko, A.E., Shapiro-Kulnane, L., and Salz, H.K. (2018). The H3K9 methyltransferase SETDB1 maintains female identity in Drosophila germ cells. Nat. Commun. *9*, 4155. https://doi.org/10.1038/s41467-018-06697-x.
9. Wang, X., Kang, J.Y., Wei, L., Yang, X., Sun, H., Yang, S., Lu, L., Yan, M., Bai, M., Chen, Y., et al. (2019). PHF7 is a novel histone H2A E3 ligase prior to histone-to-protamine exchange during spermiogenesis. Development *146*, dev175547. https://doi.org/10.1242/dev.175547.
10. Geis, F.K., and Goff, S.P. (2020). Silencing and Transcriptional Regulation of Endogenous Retroviruses: An Overview. Viruses *12*. https://doi.org/10.3390/v12080884.
11. Johnson, W.E. (2019). Origins and evolutionary consequences of ancient endogenous retroviruses. Nat. Rev. Microbiol. *17*, 355–370. https://doi.org/10.1038/s41579-019-0189-2.
12. Sakashita, A., Maezawa, S., Takahashi, K., Alavattam, K.G., Yukawa, M., Hu, Y.C., Kojima, S., Parrish, N.F., Barski, A., Pavlicev, M., and Namekawa, S.H. (2020). Endogenous retroviruses drive species-specific germline transcriptomes in mammals. Nat. Struct. Mol. Biol. *27*, 967–977. https://doi.org/10.1038/s41594-020-0487-4.
13. Kim, C.R., Noda, T., Kim, H., Kim, G., Park, S., Na, Y., Oura, S., Shimada, K., Bang, I., Ahn, J.Y., et al. (2020). PHF7 Modulates BRDT Stability and Histone-to-Protamine Exchange during Spermiogenesis. Cell Rep. *32*, 107950. https://doi.org/10.1016/j.celrep.2020.107950.
14. Maezawa, S., Yukawa, M., Alavattam, K.G., Barski, A., and Namekawa, S.H. (2018). Dynamic reorganization of open chromatin underlies diverse transcriptomes during spermatogenesis. Nucleic Acids Res. *46*, 593–608. https://doi.org/10.1093/nar/gkx1052.
15. Ito, J., Gifford, R.J., and Sato, K. (2020). Retroviruses drive the rapid evolution of mammalian APOBEC3 genes. Proc. Natl. Acad. Sci. USA *117*, 610–618. https://doi.org/10.1073/pnas.1914183116.
16. Medjakovic, S., Mueller, M., and Jungbauer, A. (2010). Potential health-modulating effects of isoflavones and metabolites via activation of PPAR and AhR. Nutrients *2*, 241–279. https://doi.org/10.3390/nu2030241.
17. Hara, S., Furukawa, F., Mukai, K., Yazawa, T., and Kitano, T. (2020). Peroxisome proliferator-activated receptor alpha is involved in the temperature-induced sex differentiation of a vertebrate. Sci. Rep. *10*, 11672. https://doi.org/10.1038/s41598-020-68594-y.
18. Monrose, M., Thirouard, L., Garcia, M., Holota, H., De Haze, A., Caira, F., Beaudoin, C., and Volle, D.H. (2021). New perspectives on PPAR, VDR and FXRα as new actors in testicular pathophysiology. Mol. Aspect. Med. *78*, 100886. https://doi.org/10.1016/j.mam.2020.100886.
19. Jia, Y., Wu, C., Kim, J., Kim, B., and Lee, S.J. (2016). Astaxanthin reduces hepatic lipid accumulations in high-fat-fed C57BL/6J mice via activation of peroxisome proliferator-activated receptor (PPAR) alpha and inhibition of PPAR gamma and Akt. J. Nutr. Biochem. *28*, 9–18. https://doi.org/10.1016/j.jnutbio.2015.09.015.
20. Sun, L., Miyaji, N., Yang, M., Mills, E.M., Taniyama, S., Uchida, T., Nikawa, T., Li, J., Shi, J., Tachibana, K., and Hirasaka, K. (2021). Astaxanthin Prevents Atrophy in Slow Muscle Fibers by Inhibiting Mitochondrial Reactive Oxygen Species via a Mitochondria-Mediated Apoptosis Pathway. Nutrients *13*, 379. https://doi.org/10.3390/nu13020379.
21. Olugbodi, J.O., Samaila, K., Lawal, B., Anunobi, O.O., Baty, R.S., Ilesanmi, O.B., and Batiha, G.E.S. (2021). Computational and Preclinical Evidence of Anti-ischemic Properties of L-Carnitine-Rich Supplement via Stimulation of Anti-inflammatory and Antioxidant Events in Testicular Torsed Rats. Oxid. Med. Cell. Longev. *2021*, 5543340. https://doi.org/10.1155/2021/5543340.
22. Yatsenko, A.N., Georgiadis, A.P., Röpke, A., Berman, A.J., Jaffe, T., Olszewska, M., Westernströer, B., Sanfilippo, J., Kurpisz, M., Rajkovic, A., et al. (2015). X-linked TEX11 mutations, meiotic arrest, and azoospermia in infertile men. N. Engl. J. Med. *372*, 2097–2107. https://doi.org/10.1056/NEJMoa1406192.
23. Ghieh, F., Mitchell, V., Mandon-Pepin, B., and Vialard, F. (2019). Genetic defects in human azoospermia. Basic Clin. Androl. *29*, 4. https://doi.org/10.1186/s12610-019-0086-6.
24. Sun, M.A., Wolf, G., Wang, Y., Senft, A.D., Ralls, S., Jin, J., Dunn-Fletcher, C.E., Muglia, L.J., and Macfarlan, T.S. (2021). Endogenous Retroviruses Drive Lineage-Specific Regulatory Evolution across Primate and Rodent Placentae. Mol. Biol. Evol. *38*, 4992–5004. https://doi.org/10.1093/molbev/msab223.
25. Davis, M.P., Carrieri, C., Saini, H.K., van Dongen, S., Leonardi, T., Bussotti, G., Monahan, J.M., Auchynnikava, T., Bitetti, A., Rappsilber, J., et al. (2017). Transposon-driven transcription is a conserved feature of vertebrate spermatogenesis and transcript evolution. EMBO Rep. *18*, 1231–1247. https://doi.org/10.15252/embr.201744059.
26. Eroglu, E., Schell, J.P., and Chien, K.R. (2021). PHF7 directs cardiac reprogramming. Nat. Cell Biol. *23*, 440–442. https://doi.org/10.1038/s41556-021-00684-z.
27. Garry, G.A., Bezprozvannaya, S., Chen, K., Zhou, H., Hashimoto, H., Morales, M.G., Liu, N., Bassel-Duby, R., and Olson, E.N. (2021). The histone reader PHF7 cooperates with the SWI/SNF complex at cardiac super enhancers to promote direct reprogramming. Nat. Cell Biol. *23*, 467–475. https://doi.org/10.1038/s41556-021-00668-z.
28. Carrell, D.T. (2019). The Sperm Epigenome: Implications for Assisted Reproductive Technologies. Adv. Exp. Med. Biol. *1166*, 47–56. https://doi.org/10.1007/978-3-030-21664-1_3.
29. Kherraf, Z.E., Cazin, C., Coutton, C., Amiri-Yekta, A., Martinez, G., Boguenet, M., Fourati Ben Mustapha, S., Kharouf, M., Gourabi, H., Hosseini, S.H., et al. (2019). Whole exome sequencing of men with multiple morphological abnormalities of the sperm flagella reveals novel homozygous QRICH2 mutations. Clin. Genet. *96*, 394–401. https://doi.org/10.1111/cge.13604.

30. Lundy, S.D. (2021). Antioxidants in male infertility. Urology. https://doi.org/10.1016/j.urology.2021.10.041.
31. Ran, F.A., Hsu, P.D., Wright, J., Agarwala, V., Scott, D.A., and Zhang, F. (2013). Genome engineering using the CRISPR-Cas9 system. Nat. Protoc. *8*, 2281–2308. https://doi.org/10.1038/nprot.2013.143.
32. Corces, M.R., Trevino, A.E., Hamilton, E.G., Greenside, P.G., Sinnott-Armstrong, N.A., Vesuna, S., Satpathy, A.T., Rubin, A.J., Montine, K.S., Wu, B., et al. (2017). An improved ATAC-seq protocol reduces background and enables interrogation of frozen tissues. Nat. Methods *14*, 959–962. https://doi.org/10.1038/nmeth.4396.
33. Kim, D., Langmead, B., and Salzberg, S.L. (2015). HISAT: A fast spliced aligner with low memory requirements(Article). Nat. Methods *12*, 357–360.
34. Li, H., Handsaker, B., Wysoker, A., Fennell, T., Ruan, J., Homer, N., Marth, G., Abecasis, G., and Durbin, R.; 1000 Genome Project Data Processing Subgroup (2009). The Sequence Alignment/Map format and SAMtools. Bioinformatics *25*, 2078–2079. https://doi.org/10.1093/bioinformatics/btp352.
35. Zhang, Y., Liu, T., Meyer, C.A., Eeckhoute, J., Johnson, D.S., Bernstein, B.E., Nusbaum, C., Myers, R.M., Brown, M., Li, W., and Liu, X.S. (2008). Model-based Analysis of ChIP-Seq (MACS). Genome Biol. *9*, R137. https://doi.org/10.1186/gb-2008-9-9-r137.
36. Landt, S.G., Marinov, G.K., Kundaje, A., Kheradpour, P., Pauli, F., Batzoglou, S., Bernstein, B.E., Bickel, P., Brown, J.B., Cayting, P., et al. (2012). ChIP-seq guidelines and practices of the ENCODE and modENCODE consortia. Genome Res. *22*, 1813–1831. https://doi.org/10.1101/gr.136184.111.
37. Wang, Q., Li, M., Wu, T., Zhan, L., Li, L., Chen, M., Xie, W., Xie, Z., Hu, E., Xu, S., and Yu, G. (2022). Exploring Epigenomic Datasets by ChIPseeker. Curr. Protoc. *2*, e585. https://doi.org/10.1002/cpz1.585.
38. Stark, R., and Brown, G. (2011). DiffBind: differential binding analysis of ChIP-Seq peak data. R Package Version 100.
39. Heinz, S., Benner, C., Spann, N., Bertolino, E., Lin, Y.C., Laslo, P., Cheng, J.X., Murre, C., Singh, H., and Glass, C.K. (2010). Simple combinations of lineage-determining transcription factors prime cis-regulatory elements required for macrophage and B cell identities. Mol. Cell *38*, 576–589. https://doi.org/10.1016/j.molcel.2010.05.004.
40. Ramírez, F., Ryan, D.P., Grüning, B., Bhardwaj, V., Kilpert, F., Richter, A.S., Heyne, S., Dündar, F., and Manke, T. (2016). deepTools2: a next generation web server for deep-sequencing data analysis. Nucleic Acids Res. *44*, W160–W165. https://doi.org/10.1093/nar/gkw257.
41. Thorvaldsdóttir, H., Robinson, J.T., and Mesirov, J.P. (2013). Integrative Genomics Viewer (IGV): high-performance genomics data visualization and exploration. Briefings Bioinf. *14*, 178–192. https://doi.org/10.1093/bib/bbs017.
42. Yu, G., Wang, L.G., Han, Y., and He, Q.Y. (2012). clusterProfiler: an R package for comparing biological themes among gene clusters. OMICS *16*, 284–287. https://doi.org/10.1089/omi.2011.0118.
43. Zhou, Y., Zhou, B., Pache, L., Chang, M., Khodabakhshi, A.H., Tanaseichuk, O., Benner, C., and Chanda, S.K. (2019). Metascape provides a biologist-oriented resource for the analysis of systems-level datasets. Nat. Commun. *10*, 1523. https://doi.org/10.1038/s41467-019-09234-6.
44. Quinlan, A.R. (2014). BEDTools: The Swiss-Army Tool for Genome Feature Analysis. Curr. Protoc. Bioinformatics *47*, 11.12.1–11.1234. https://doi.org/10.1002/0471250953.bi1112s47.
45. Wu, T., Hu, E., Xu, S., Chen, M., Guo, P., Dai, Z., Feng, T., Zhou, L., Tang, W., Zhan, L., et al. (2021). clusterProfiler 4.0: A universal enrichment tool for interpreting omics data. Innovation *2*, 100141. https://doi.org/10.1016/j.xinn.2021.100141.

STAR★METHODS

KEY RESOURCES TABLE

REAGENT or RESOURCE	SOURCE	IDENTIFIER
Antibodies		
Rabbit Polyclonal to PHF7	Invitrogen	PA5-69219
Rabbit polyclonal to PPAR alpha	abcam	Ab61182
Rabbit Polyclonal to Ah Receptor	Immunoway	YT0145
α-Tubulin Mouse Monoclonal	CST	3873S
Rabbit Lamin B1 Polyclonal	bioss	bs-1840R
Biological samples		
Human testis tissues	Peking University Third Hospital	N/A
Critical commercial assays		
ROS assay kit	Beyotime	S0033
TUNEL Apoptosis Assay Kit	Beyotime	C1086
BCA Protein Assay Kits	Thermo	23227
High-Sensitivity ChIP Kit	abcam	ab185913
Chemicals, peptides, and recombinant proteins		
Trizol	Invitrogen	15596018
RevertAid First Strand cDNA	Thermo	K1622
ABI PowerUp SYBR Green	Applied biosystems	A25742
astaxanthin	solarbio	A9241
Deposited data		
RNA-seq data	https://www.ncbi.nlm.nih.gov/geo/	GSE119701
ChIP-Seq data	https://www.ncbi.nlm.nih.gov/geo/	(GSE112912)
Experimental models: Cell lines		
Phf7 gene knockout mouse	Cyagen Biosciences	N/A
Male germ cell lines GC-1spg	procell	CL-0600
Male germ cell lines GC-2	procell	CL-0593
Software and algorithms		
ImageJ	ImageJ	https://ImageJ.nih.gov/ij/
GraphPad Prism 8.0	GraphPad	www.graphpad.com
Adobe Illustrator 2020	Adobe	http://aotucad2.xmjfg.com/pg/230.html

RESOURCE AVAILABILITY

Lead contact

Further information and requests for resources and reagents should be directed to and will be fulfilled by the lead contact, Haocheng Lin (haochenglin292@163.com).

Materials availability

This study did not generate new unique reagents.

Data and code availability

This paper analyses existing, publicly available data. The accession numbers for these datasets are listed in the key resources table.
All other data reported in this paper will be shared by the lead contact upon request.
This paper does not report original code. Any additional information required to reanalyse the data reported in this paper is available from the lead contact upon request.

EXPERIMENTAL MODEL AND SUBJECT DETAILS

Animal use and care

All animal studies were approved by the Biomedical Ethics Committee and the Animal Care and Use Committee of Peking University. The Phf7 gene knockout mouse model was created using Cyagen Biosciences (Suzhou, China). Female and male mice with Phf7 knockout heterozygotes were hybridized and homozygous mice were bred. Genomic DNA was isolated from mouse tail fragments, and genotyping was performed using polymerase chain reaction (PCR). The primer sequences used for genotype identification are listed in Table S1. All mice were raised under standard laboratory conditions with a 12 h light/dark cycle and free access to food and water. For the *in vivo* study, Phf7$^{-/-}$ mice were oral administrated with astaxanthin; 30 g mice were treated with 30 mg/kg of astaxanthin in 200 μL corn oil, with six replicates per treatment. Control mice were treated with the same volume of the solution throughout the experiment. Astaxanthin was provided by FARMNAN Biopharmaceutical (Shenzhen) Co., Ltd. (Shenzhen, China). Phenotypic changes in mouse sperm were detected after 4 weeks.

Generation of ERV-MTD knockout cell lines

ERV-MTD knockout cell line was established using the CRISPR gene editing system obtained from Professor Zhang Feng.[31] Briefly, according to a published protocol, four guide RNAs (sgRNAs) targeting the mouse ERV-MTD-838849 (chr15:85759279-85759583) region (Table S1) were designed. The experimental germline cells, including GC1 and GC2, were infected with lentivirus, selected by puromycin, and transfected with HitransG/P transfection reagent (REVG0058, Genechem). Monoclonal cells were selected using the limited dilution method and cultured for 6–14 days to obtain the genomic DNA of a single colony, which was verified by PCR, and the mutation sites were sequenced using the primers listed in Table S1. Mouse germline cells were cultured in dishes coated with poly-D-lysine/laminin (Corning) in Dulbecco's modified Eagle's medium supplemented with 10% fetal bovine serum and 1% penicillin-streptomycin at 37°C under 5% CO_2. All reagents required for cell culture are from Hyclone.

Human samples

The study was approved by the Medical Ethics Committee of the Peking University Third Hospital (2017sz-048). Patients with idiopathic azoospermia (no sperm in the ejaculate even after centrifugation) and fertile male controls (with at least natural bred one child) were recruited from the Department of Reproductive Medicine Center at Peking University Third Hospital. All patients underwent semen analysis on at least three different occasions, and those with a history of orchitis, vas deferens obstruction, or endocrine disorder were excluded. For two patients with confirmed Phf7 mutations, we further obtained a testicular biopsy. Genomic DNA was prepared from the blood samples, and exon sequencing was performed. All participants signed an informed consent form.

METHOD DETAILS

RNA extraction and reverse transcriptase polymerase chain reaction (RT-PCR)

Total RNA was extracted from the testes and cells using Trizol reagent (Invitrogen) according to the manufacturer's instructions. cDNA was synthesized using a Revertaid First Strand cDNA Synthesis Kit (Applied biosystem, k1622). cDNA was amplified by PCR using primer sets for the target and housekeeping genes. Powerup SYBR Green master mix was used according to the manufacturer's instructions (Applied Biosystems, a25742) and the QuantStudio 6 Flex System (Applied Biosystems) was used for quantitative PCR (q-PCR). PCR cycle consisted of denaturation for 45 s at 94°C, annealing for 1 min at 55°C, and extension for 1 min 30 s at 72°C. The primer sequences used for qPCR analysis are listed in Table S1. All RT-PCR primers were designed according to sequences obtained from GenBank and synthesized using Genepharma Biotech (Suzhou, China).

Sperm isolation and computer-assisted sperm analysis (CASA)

Sperms were harvested by dissecting and cutting the cauda epididymis. Briefly, Ham's F10 medium was preheated at 37°C supplemented with 25 mm HEPES and 4 mg/mL bovine serum albumin. The epididymal tail was washed in Ham's F10 medium, cut, and released into 1 mL Ham's F10 medium using scissors, and further gently filtered through 70 μm filter to remove tissue fragments. The culture medium containing sperm was placed into a calibrated slide. Sperm counting and sperm activity analysis were performed using CASA.

Histology and immunohistochemical staining

Testicular and epididymal tissues were fixed in Bouin's fixative for 24 h, embedded in paraffin, and sectioned. Before staining, 5 μm paraffin sections were dewaxed in xylene, rehydrated by reducing the concentration of ethanol, and washed in distilled water. The sections were stained with Hematoxylin and Eosin. For immunostaining, 5 μm paraffin-embedded sections of testes were used for staining Phf7. After deparaffinization and rehydration, slides were incubated with boiling 0.01 M sodium citrate (pH 6.0) for 10 min to retrieve the antigens before immunostaining. Standard immunostaining was then performed.

Terminal deoxynucleotidyl transferase dUTP nick-end labeling (TUNEL) and reactive oxygen species (ROS)

For apoptosis analysis, firstly, testes were fixed with optimal cutting temperature compound and 8 μm frozen sections were taken. The Colorimetric TUNEL Apoptosis Assay Kit was then used for the analysis (Beyotime Biotech C1091). ROS analysis was performed using ROS assay kit (Beyotime S0033s).

Scanning electron microscopy

Sperm cells were fixed in 2.5% glutaraldehyde solution at room temperature for 2 h and stored at 4°C. The sperm cells were collected by centrifugation and washed thrice with PBS. The samples were then fixed with 1% osmium tetroxide for 15 min. After PBS cleaning, the samples were collected and dried. The sperm cells were clinging to the double-sided adhesive of conductive carbon film. They were placed on the sample table of the ion sputtering instrument, sprayed with gold for 30 s, and examined using a transmission electron microscope.

Immunofluorescence staining

Cells on the glass and tissue sections were fixed with 4% paraformaldehyde in PBS for 15 min at room temperature, followed by three times washing with PBS every 5 min. The samples were then blocked with permeabilizing buffer (1% Triton X-100) for 1 h. All primary antibodies were diluted with blocking buffer and incubated with samples overnight at 4°C, followed by three times washing with PBS every 5 min. The samples were treated with a secondary antibody coupled with fluorescence for 1 h in the dark at room temperature. The nuclei were stained with 4′,6-diamidino-2-phenylindole (DAPI) for 10 min. Laser confocal scanning images were captured using a ZEISS inverted spectral confocal microscope.

Western blot analysis

Testes and cells were lysed in Radio Immunoprecipitation Assay lysis buffer (Beyotime Biotech, P0028) with protease inhibitor phenylmethylsulfonyl fluoride (Beyotime Biotech, ST505), and the protein concentration was measured using a bicinchoninic acid Protein Assay Kit (Thermo Scientific, A55865). The samples were loaded onto sodium dodecyl sulfate-polyacrylamide gel electrophoresis and transferred to a polyvinylidene fluoride membrane (Millipore), which was blocked in 5% milk and probed with primary antibodies, and subsequent horseradish peroxidase (HRP)-linked secondary antibodies. HRP activity was detected using pierce enhanced chemiluminescence western blotting substrate detection kit (Thermo Scientific,3 4095). The intensity of a specific strip was scanned using image analysis software in the laboratory.

ChIP-qPCR analysis

The chromatin immunoprecipitation (ChIP) procedure was performed using the High-Sensitivity ChIP Kit (ab185913) following the manufacturer's instructions. 2 μg antibodies against PHF7 (Invitrogen) or Histone H3K4me3 (Active motif), isotype IgG used as negative control were added and the complex co-precipitates are captured by Protein G magnetic beads. Genomic DNA pellets were purified using phenol-chloroform extraction and ethanol precipitation, then resuspended in 20 μL water, which is ready for PCR. Relative enrichment was calculated as the amount of amplified DNA relative to values obtained after normal IgG immunoprecipitation. The primers used are listed below.

Assay for transposase-accessible chromatin using sequencing (ATAC-seq) analysis

ATAC-seq was performed as previously reported,[32] two mice were used in each group of Phf7$^{-/-}$ and wild-type (WT) groups. Nuclei were extracted from the testicular tissue samples, and the nuclear pellet was resuspended in Tn5 transposase reaction mix. The transposition reaction was incubated at 37°C for 30 min. Equimolar amounts of Adapter 1 and Adatper 2 were added after transposition, and PCR was performed to amplify the library. After the PCR reaction, libraries were purified with AMPure beads, and library quality was assessed using Qubit. The library preparations were sequenced on an Illumina HiSeq platform and 150 bp paired-end reads were generated.

The adaptor sequences were trimmed from the reads using Trim Galore (https://github.com/FelixKrueger/TrimGalore/releases). These reads were aligned to a reference genome using HISAT2 (http://github.com/infphilo/hisat2)[33] with standard parameters. SAMtools 1.16[34] was used to convert the comparison files into bam format, and Picard (http://broadinstitute.github.io/picard/) was used to delete the duplicates generated by PCR of the above file to obtain clean reads. All peak calling was performed using model-based analysis of chip-seq (MACS2).[35] To identify enriched regions from biologically replicated samples in Phf7$^{-/-}$ ATAC-seq, we used the Irreproducible Discovery Rate (IDR) method (https://github.com/nboley/idr),[36] where the parameter setting of MACS2 should not be too strict to identify more peaks. Following this method, peak calling was performed using MACS2 with relaxed conditions (–shift −100 –extsize 200 –nomodel -B –SPMR -gmm) on each of the two replicates of the pooled dataset. IDR analysis was then performed, and reproducibility was checked. To obtain the final peak sets, the data were sorted by -log10 (p value). The threshold recommended by the authors was used. The peaks were annotated and visualized using the R package ChIPseeker.[37] R package DiffBind[38] was used to find the difference in peaks between the Phf7$^{-/-}$ and wild-type (WT) groups, with | fold change| $\geq$ 2 and false discovery rate (FDR) $\leq$ 0.01. Motif calling was performed using the Homer command annotate Peaks and Homer command find Motifs Genome (http://homer.ucsd.edu/homer/motif/) with parameter "-size 200 and -len 8, 10, and 12".[39]

RNA-seq analysis

RNA-seq (GSE119701) and chromatin immunoprecipitation sequencing (ChIP-Seq) (GSE112912) data were obtained from the Gene Expression Omnibus (https://www.ncbi.nlm.nih.gov/geo/).[9] The reads were mapped against the Mus musculus GRCm38. The RNA-seq data were processed in this study, and the analysis process included quality control, mapping, and filtering.

Differential expression analysis

Sequence alignments were processed using DESeq2 software (http://bioconductor.org/packages/DESeq2/) to quantify the expression levels and analyze differentially expressed genes. H3K4me3-ChIP-seq sequencing files were processed in the same way as the ATAC-seq files,

where peak calls used MACS2. To show the ChIP binding signal surrounding Transcriptional Start Sites (TSSs) or gene bodies, alignments were converted into bigWig tracks using the bamCoverage function implemented in DeepTools[40] and used for visual inspection with the Integrative Genomics Viewer genome browser.[41] Gene set enrichment analysis was performed using R package clusterProfiler[42] and Metascape (http://metascape.org).[43]

ERV analysis

A mouse RepeatMasker file was downloaded from the UCSC database. A Python script was written to extract the location information of the ERV from the downloaded files. The above-mentioned files were organized into annotated files to calculate the ERV expression. To identify the ERV of each location, we assigned an identification ID to each ERV element. Differentially expressed ERVs were analyzed using DeSeq2. ERV provides a promoter and also acts as an enhancer to affect the expression of surrounding genes. Gene annotation files and ERV sequence location files were used to identify genes that overlapped with ERV, including those overlapping with promoter regions, using BEDtools.[44]

QUANTIFICATION AND STATISTICAL ANALYSIS

All quantitative biochemical data were representative of at least three independent experiments. For statistical comparisons, all data were first subjected to a Gaussian distribution test. Only the data with normal distribution and similar variances between groups were used for comparison and parametric statistical test. A two-tailed unpaired t test was used to compare the mean values between two groups and overlapping enrichment significance was calculated using Fisher's exact test. Prism software (GraphPad 8.0) was used to generate graphs and analyze the data. ClusterProfiler (version 4.0.5)[45] and Metascape (http://metascape.org)[43] were used for Gene Ontology (GO) enrichment analyses.